American Genetic Association

Journal of Heredity, 2019, 684–695
doi:10.1093/jhered/esz045
Original Article
Advance Access publication July 11, 2019

OXFORD

Original Article

Genomic Signatures of Selection along a Climatic Gradient in the Northern Range Margin of the White-Footed Mouse (*Peromyscus leucopus*)

Alan Garcia-Elfring, Rowan D. H. Barrett,* and Virginie Millien*

From the Redpath Museum, McGill University, 859 Sherbrooke Street West, Montreal, QC, Canada H3A OC4 and the Department of Biology, McGill University, 859 Sherbrooke Street West, Montreal, QC, Canada H3A OC4.

Address correspondence to Alan Garcia-Elfring, Redpath Museum, McGill University, 859 Sherbrooke Street West, Montreal, QC, Canada H3A OC4, or email: alan.garcia-elfring@mail.mcgill.ca.

Received November 19, 2018; First decision December 30, 2018; Accepted July 10, 2019.

Corresponding Editor: Kim Andrews

*These authors contributed equally to the work.

Abstract

Identifying genetic variation involved in thermal adaptation is likely to yield insights into how species adapt to different climates. Physiological and behavioral responses associated with overwintering (e.g., torpor) are thought to serve important functions in climate adaptation. In this study, we use 2 isolated *Peromyscus leucopus* lineages on the northern margin of the species range to identify single nucleotide polymorphisms (SNPs) showing a strong environmental association and test for evidence of parallel evolution. We found signatures of clinal selection in each lineage, but evidence of parallelism was limited, with only 2 SNPs showing parallel allele frequencies across transects. These parallel SNPs map to a gene involved in protection against iron-dependent oxidative stress (*Fxn*) and to a gene with unknown function but containing a forkhead-associated domain (*Fhad1*). Furthermore, within transects, we find significant clinal patterns in genes enriched for functions associated with glycogen homeostasis, synaptic function, intracellular Ca^{2+} balance, H3 histone modification, as well as the G2/M transition of cell division. Our results are consistent with recent literature on the cellular and molecular basis of climate adaptation in small mammals and provide candidate genomic regions for further study.

Keywords: climate adaptation, *Peromyscus*, population genomics, RAD-seq, torpor

Understanding the role that the thermal environment plays in shaping local adaptation and global biodiversity is a burgeoning area of research (Johnston and Bennett 2008; Keller and Seehausen 2012; Araújo et al. 2013; Porcelli et al. 2015; Chen et al. 2018). Animals in temperate regions face particular climatic challenges as they must be adapted to cope with seasonal fluctuations in temperature and food availability. To survive low winter temperature and scarce resources, many species have evolved the ability to decrease energy expenditure through torpor, a highly common strategy among small mammals entailing precise regulation of metabolic rate (Lyman et al. 1982). Small mammals, having a high surface area to volume ratio, are particularly susceptible to heat loss during cold stress. This energetic constraint imposed by ambient temperature and lack of energy resources drives adaptation in small mammals, in part, through shifts

in metabolism (Humphries et al. 2002; Lovegrove 2003; Rezende et al. 2004; Fristoe et al. 2015). Understanding the genomic basis of thermal adaptation may yield insights about the targets of selection that can allow species to adapt to ongoing global climate change. In this regard, populations on the margins of temperature-limited distributions provide an opportunity to study adaptation to novel thermal regimes (Hill et al. 2011).

Population genomic methods are often used to search for evidence of local adaptation in natural populations by scanning the genome for the signature of positive selection (e.g., White et al. 2013; Fumagalli et al. 2015; Babin et al. 2017; Bassham et al. 2018). However, it is well recognized that stochastic processes can cause similar patterns to those arising from selection (Currat et al. 2006; Gilbert et al. 2017). One potential solution to discriminating between stochastic and deterministic scenarios is to investigate independent instances of populations in similar environments undergoing local adaptation (e.g., Bassham et al. 2018). Because large allele frequency changes caused by genetic drift should occur at random single nucleotide polymorphism (SNP) loci across the genome, identifying the same outlier SNPs in multiple populations experiencing the same selection regime, that is, parallel evolution, can provide evidence for natural selection.

Peromyscus leucopus is a geographically widespread rodent species native to eastern North America. The northern range limit of *P. leucopus* reaches southern Quebec, where it is ecologically limited by cold-winter temperature (Roy-Dufresne et al. 2013). The St. Lawrence River separates 2 postglacial *P. leucopus* lineages (Fiset et al. 2015; Garcia-Elfring et al. 2017) that over recent decades have been expanding northward (Roy-Dufresne et al. 2013) into latitudes inhabited by the more cold-adapted *Peromyscus maniculatus*. Relative to *P. leucopus*, *P. maniculatus* has behavioral and metabolic traits more suitable for colder winters. While both species may share similar thresholds under which they become torpid, approximately 4.5 °C (Tannenbaum and Pivorun 1988), their torpor response is different in important ways. For example, in response to cold-stress, *P. leucopus* builds less insulated nests, hoards less food, and is less likely to become torpid under caloric restriction, relative to *P. maniculatus* (Tannenbaum and Pivorun 1988; Pierce and Vogt 1993). Within *P. leucopus*, there is also a latitudinal gradient in the torpor response to environmental cues. Heath and Lynch (1983) studied laboratory-reared *P. leucopus* lines from wild mice caught in 2 states with different winter climates, Georgia and Connecticut. They found that mice belonging to the lineage from Connecticut, where the winter is colder and longer, were more likely to become torpid in response to cold temperature and a short photoperiod. More recently, genomic data from hibernating 13-lined ground squirrels (*Ictidomys tridecemlineatus*) indicates variation in the onset of hibernation is genetically controlled and highly heritable (Grabek et al. 2017). Thus, if thermal adaptation occurs through changes in metabolic and behavioral responses to local (winter) temperature, then genes involved in energy metabolism and neural circuitry should be overrepresented in SNPs showing the signature of clinal selection.

Here, we investigate the genomic signature of clinal selection in *P. leucopus* inhabiting a climatic gradient (Table 1) in southern Quebec. We study 2 independent lineages of *P. leucopus*, and ask: do these lineages show patterns of clinal genetic variation that deviate from neutrality? If so, do we find parallelism across lineages? What are the functions of genes showing clinal patterns in allele frequency? With ongoing climate change around the world, answering such questions will advance our understanding of the phenotypes under selection in small mammals facing novel thermal regimes.

Materials and Methods

Study System and DNA Extraction

We collected *P. leucopus* samples from southern Quebec during the summer of 2013 and 2014, as described in Garcia-Elfring et al. (2017). Here, we use 47 *P. leucopus* samples from 3 sites north of the St. Lawrence River ("transect A" hereafter; sites: A1 [n = 16], A2 [n = 11], and A3 [n = 20]) and 68 samples from 4 sites south of the St. Lawrence River ("transect B" hereafter; sites: B1 [n = 20], B2 [n = 8], B3 [n = 20], and B4 [n = 20]). We previously used genome-wide markers to investigate population structure (Garcia-Elfring et al. 2017) and established that the St. Lawrence River is a strong barrier to gene-flow that separates lineages expanding from distinct source populations or glacial refugia (Rowe et al. 2006; Fiset et al. 2015). We now look for selection in 2 of these lineages using populations along a climatic gradient (Table 1). These populations are labeled according to transect and in ascending order going north (Figure 1). Within transects, our collection sites consist of relatively small forest patches scattered in an area dominated by agricultural fields that are relatively ineffective barriers to gene-flow (Marrotte et al. 2014). These populations thus provide an opportunity to look for evidence of clinal selection within and across lineages. DNA was extracted from liver or muscle tissue using a standard 3-day phenol-chloroform extraction protocol (Sambrook et al. 1989). Samples were identified as *P. leucopus* by PCR amplification of a mitochondrial COIII sequence (Tessier et al. 2004).

Table 1. Summary information of collection sites and the local winter climate (years 2001–2010)

Site	n	Latitude	Longitude	Elevation (m)	Average minimum winter temperature	Average maximum winter temperature	Average minimum January temperature	Winter degree—days below 0	MAT	MAP	DD > 5	CMD
A1	19	45.33	−74.4	80	−12.3	−1.8	−14	668	6.5	986	2132	125
A3	11	46.07	−73.28	24	−13.5	−2.9	−15.5	763	6	1076	2066	98
A4	20	46.3	−73.09	63	−14	−3.4	−16.2	803	5.6	1103	1990	75
B1	20	45.06	−73.29	46	−11	0.1	−12.7	557	7.4	946	2257	114
B2	8	45.42	−73.07	46	−12	−1	−13.7	626	6.9	1071	2183	78
B3	20	45.66	−72.75	79	−12.7	−1.9	−14.6	688	6.4	1125	2105	62
B4	20	45.87	−72.56	88	−13.2	−2.7	−15.4	746	5.9	1122	2030	51

Included are annual climatic variables, such mean annual temperature (MAT) and precipitation (MAP), degree-days above 5 °C (DD > 5), and the Hargreaves moisture deficit (CMD, measures evapotranspiration), all of which covary. The temperatures are in degrees Celsius.

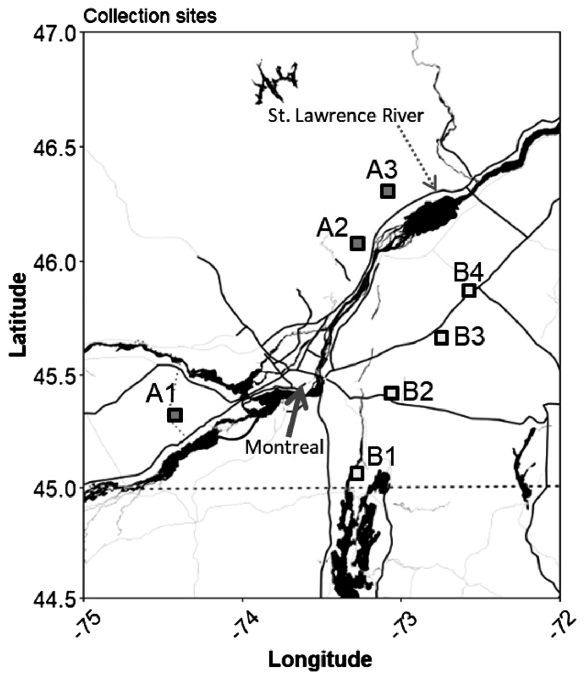

Figure 1. Geographical locations of *Peromyscus leucopus* populations sampled in southern Quebec. Three populations were sampled north of the St. Lawrence River (transect A), sites A1 ($n = 16$), A2 ($n = 11$), and A3 ($n = 20$). Four populations were sampled south of the St. Lawrence River in transect B. These sites include B1 ($n = 20$), B2 ($n = 8$), and B3 ($n = 20$), and B4 ($n = 20$). The bold dotted line demarks international border, light dotted line demarks the provincial border.

Sequencing Restriction-Site Associated DNA Libraries

RAD-seq library preparation was done at the Institut de biologie intégrative et des systèmes (IBIS) at Université Laval using a modified version of the genotyping-by-sequencing protocol (Elshire et al. 2011). Briefly, we used the rare cutting (1 cut/4096 bp) restriction enzyme *Pst*I (CTGCAG) to anchor markers and the more frequent cutting (1 cut/256 bp) *Msp*I (CCGG) to define library size. Once ligation of barcoded and common adapters was completed, size selection was done with PCR to pools of 48 samples. We sequenced 100 bp paired-end reads on the Illumina HiSeq 2000 platform at the Genome Quebec Innovation Center using one lane per 48 individuals.

SNP Genotyping and Bioinformatics

We processed raw data and identified SNPs using Stacks 1.48 (Catchen et al. 2013), a pipeline designed for short-read sequences. Raw reads were demultiplexed and quality filtered using the *process_radtags* script, which discarded reads of low quality (-q) and with uncalled bases (-c). We then aligned demultiplexed reads to the *Peromyscus maniculatus bairdii* reference genome (Pman_1.0) assembled at the unplaced scaffold level using Bowtie2 2.3.4.1 (Langmead and Salzberg 2012) with end-to-end alignment and default parameters. We discarded ambiguously mapped reads with SAMtools (Li et al. 2009) by removing reads with low mapping quality (-q 20). We identified SNPs with a minimum depth of coverage of 5 reads per allele (-m 5) using the *ref_map.pl* wrapper program from Stacks. This resulted in a catalogue with 1 101 363 RAD loci. From this catalogue, 2 SNP data sets were obtained with the *populations* script, one for each transect. Filters required each SNP have a minimum allele frequency of at least 5% (--min_maf 0.05, applied globally at the metapopulation level) and a maximum heterozygosity of 0.50 (--max_obs_het 0.50) to avoid paralogs. Each SNP was genotyped in every population within each of the 2 transects (-p 3 and 4) and in at least 70% of individuals within each population (-r 0.70). We used one SNP per RAD locus to avoid linkage bias. For repeatability, only the first SNP per RAD locus (--write_single_snp) was analyzed (e.g., Combosch et al. 2017; Nunziata and Weisrock 2018; De Candia et al. 2019). This resulted in 21 723 SNPs for transect A and 79 956 SNPs for transect B. However, we identified some SNPs that were duplicates under a distinct catalogue ID assigned by Stacks. We removed the duplicates and retained SNPs with unique genomic locations (scaffold and SNP position), ending with 21 505 SNPs for transect A and 79 343 SNPs for transect B. Between these 2 data sets, 14 687 are "shared SNPs." The catalogue locus ID for these markers (21 505 SNPs for transect A and 79 343 SNPs for transect B) were incorporated in a text file ("whitelist") used by the *populations* script to obtain population genetic information for these SNPs only. We used the same approach to obtain allele frequency information for candidates under selection.

We used the software *LinkImpute* (Money et al. 2015) to impute the 18.6% missing data in transect A and the 14.8% missing in transect B. *LinkImpute* was designed for unordered RAD-seq data and uses correlations between markers and a *k*-nearest neighbor algorithm ("LD-kNNi") to impute genotypes. We obtained imputation accuracies of 0.846 for transect A and 0.836 for transect B.

Genetic Variation, Population Structure, and Linkage Disequilibrium

We obtained measures of genetic diversity (observed and expected heterozygosity, π, and F_{IS}) for populations within each transect using the *populations* script. We estimated genome-wide divergence (F_{ST}) with the software *genepop* (Rousset 2008), implemented in R 3.5.1 (R Core Team 2016). To test for significant divergence, we used the *test_diff* function which uses Fisher's method to evaluate whether alleles are drawn from the same distribution in each pairwise comparison. We also summarized genetic variation with a principal component analysis (PCA) using the R package *LEA* (Frichot and François 2015).

Identifying Candidate SNPs for Local Adaptation

We combined 2 genome scan approaches to identify SNPs potentially under clinal selection. Both approaches compare the distribution of allele frequencies relative to a neutral model (Lewontin and Krakauer 1973; Beaumont and Nichols 1996). We used the program *pcadapt* 4.0 (Luu et al. 2017) to look for SNPs showing evidence of local adaptation. This program ascertains population structure with K principal components (PCs) and identifies SNPs strongly associated with this captured population structure, as measured by a vector of K Z-scores. Relative to 3 other genome scan programs, *pcadapt* was found to be the most powerful method under a model of range expansion (Luu et al. 2017). We used the scree plot of a PCA to estimate the number of PCs to ascertain population structure, testing 20 PCs in transect A and 30 in transect B (Supplementary Figures S1 and S2). However, our decision was ultimately based on having a well-calibrated null hypothesis, demonstrated by a histogram with uniform P values and a peak near zero. We plotted histograms for the first 2, 3, 4, and 5 PCs and selected 3 PCs as it showed the best calibrated histogram for

both transects (Supplementary Figures S3 and S4). Having well-calibrated *P* values is an indication that confounding factors (e.g., genetic drift, isolation-by-distance) have been properly taken into account (François et al. 2016). We used 3 PCs to capture population structure in both transects. The test statistic employed by *pcadapt* to identify candidate SNPs is the Mahalanobis distance. We corrected for multiple hypothesis testing with the false discovery rate (FDR) method of Storey and Tibshirani (2003), implemented in the R package *qvalue* (Storey et al. 2018). We applied a FDR threshold of 0.10 to identify candidate SNPs.

Our second approach for detecting candidates under selection involved testing for clinal variation deviating from neutrality along an environmental variable (e.g., Haldane 1948; Waldvogel et al. 2018). To do this, we applied latent factor mixed models (*LFMM*; Frichot et al. 2013) using the package *LEA* (Frichot and François 2015) and tested for SNPs with allele frequencies significantly associated with winter climate, the range-limiting factor. Comparative studies have shown *LFMM* provides a good trade-off between power and error rate and performs well under a variety of sampling schemes (De Villemereuil et al. 2014: Lotterhos and Whitlock 2015). *LFMM* accounts for population structure using statistical models called latent factors. These random factors attempt to control for the confounding effects of population structure and isolation by distance (Frichot et al. 2013; François et al. 2016). The choice of how many latent factors to use was informed by the number of genetic clusters present in the data set, which we evaluated using the computer program *sNMF* (Frichot et al. 2014) and the minimal cross-entropy criterion implemented in *LEA*. Two latent factors were used in both transects (Supplementary Figures S5 and S6). *LFMM* is based on a Markov Chain Monte Carlo approach and uses the Gibbs sampling algorithm for parameter estimation. We applied 15 repetitions of 20 000 iterations with 10 000 for burn-in. We combined the *Z* scores from the 15 repetitions and computed the median. We then recalibrated *Z* scores by dividing by the inflation factor before computing the *P* values displayed in the histogram (Supplementary Figures S7 and S8). We accounted for multiple testing using the *q* value procedure and a FDR of 0.10. We obtained climate data for the most recent decade (2001–2010) available using the platform ClimateNA (Wang et al. 2016). Winter climate, which limits the range of *P. leucopus*, was summarized with 4 variables: average minimum and maximum winter temperature, average minimum temperature during the coldest month of the year (January), and winter degree-days below 0 °C (Table 1). Altitude estimates for each site were obtained from the online platform Geoplaner V2.8 (data from Google Elevation Service) and incorporated into ClimateNA to estimate temperature. We reduced winter climate data to a single dimension by log-transforming absolute values and running a PCA (centered and scaled) with the prcomp function in base R. The first PC, which explained all the variance (Supplementary Figure S9), was treated as the environmental variable.

SNP Annotation and Gene Ontology Enrichment Analysis

To annotate SNPs, we applied a custom bash script that used the genomic location of each marker (scaffold and SNP position) and gene intervals from the annotation file (.gff3) of the Pman_1.0 reference genome to map SNPs to protein-coding genes ("gene_biotype=protein_coding"). We investigated the enrichment of GO terms with the use of the software *topGO* (Alexa and Rahnenfuhrer 2016). We first retrieved gene attributes ("go_id" and "external_gene_name") from the Pman_1.0 database on ensembl (Zerbino et al. 2017) using the package *biomaRT* (Durinck et al. 2005; Durinck et al. 2009). To test for overrepresentation of biological processes in candidate SNPs, we used the "classic" algorithm, which tests each GO term independently, and Fisher's exact (Alexa and Rahnenfuhrer 2016). Within each transect, the GO analysis was based on a comparison between the list of candidate genes under clinal selection and the list of genes present in the respective SNP dataset ("gene universe," Alexa and Rahnenfuhrer 2016). To avoid false positives, we required a minimum of 5 nodes per GO term (i.e., 5 genes annotated per GO term).

Results

Genetic Diversity and Population Structure

Overall, we find slightly less genetic variation in individuals from transect A (north of the St. Lawrence River) than in individuals from transect B (Table 2). However, we find that the northern-most site (i.e., A3) shows relatively low F_{IS}, or excess heterozygosity, perhaps due to out-crossing with an unsampled population. Genome-wide levels of F_{ST} range from 0.057 (A2–A3) to 0.101 (A1–A3) in transect A (mean: 0.075, Supplementary Table S1), and from 0.037 (B3–B4) to 0.070 (B1–B4) in transect B (mean: 0.052, Supplementary Table S2). We evaluated whether alleles across all SNPs are drawn from the same distribution in each pairwise comparison to test for significant divergence. The result was "highly significant" for all pairwise comparisons (Supplementary Tables S1 and S2). A highly significant result is reported when a test yields a zero *P* value estimate (Rousset 2019). PCA on genomic variation also shows that individuals generally cluster according to sampling locality (Figure 2).

Outlier SNPs

Using *pcadapt*, we detected 598 (2.8%) candidate SNPs in transect A and 1177 (1.5%) in transect B (referred to as "*pcadapt*-outliers" hereafter). With *LFMM*, 281 SNPs (1.3%) showed a significant gene–environment correlation in transect A and 529 SNPs (0.67%) in transect B ("*LFMM*-outliers" hereafter). Within transects, looking for overlap between methods we find 37 in transect A (0.17%) and 137 (0.17%) in transect B ("*pcadapt-LFMM*-outliers" hereafter). We found no overlap of *pcadapt-LFMM*-outliers across transects. However, traits under climate-induced selection may be polygenic and selection reflected as subtle shifts in allele frequency at individual SNPs. Thus, requiring that a SNP be a candidate in *pcadapt* and *LFMM* may be overly conservative as it requires that SNPs show relatively large differences in allele frequency, in addition to a significant association with the environment. We therefore also looked for parallelism among *LFMM*-outlier SNPs. First, we found that

Table 2. Measures of expected heterozygosity (H_e), observed heterozygosity (H_o), nucleotide diversity (π), and the inbreeding coefficient (F_{IS}) for each collection site across all SNPs

Site ID	H_o	H_e	π	F_{IS}
A1	0.184	0.260	0.271	0.252
A2	0.148	0.235	0.250	0.269
A3	0.239	0.250	0.257	0.057
B1	0.234	0.267	0.275	0.118
B2	0.237	0.253	0.272	0.086
B3	0.221	0.259	0.267	0.134
B4	0.223	0.260	0.268	0.130

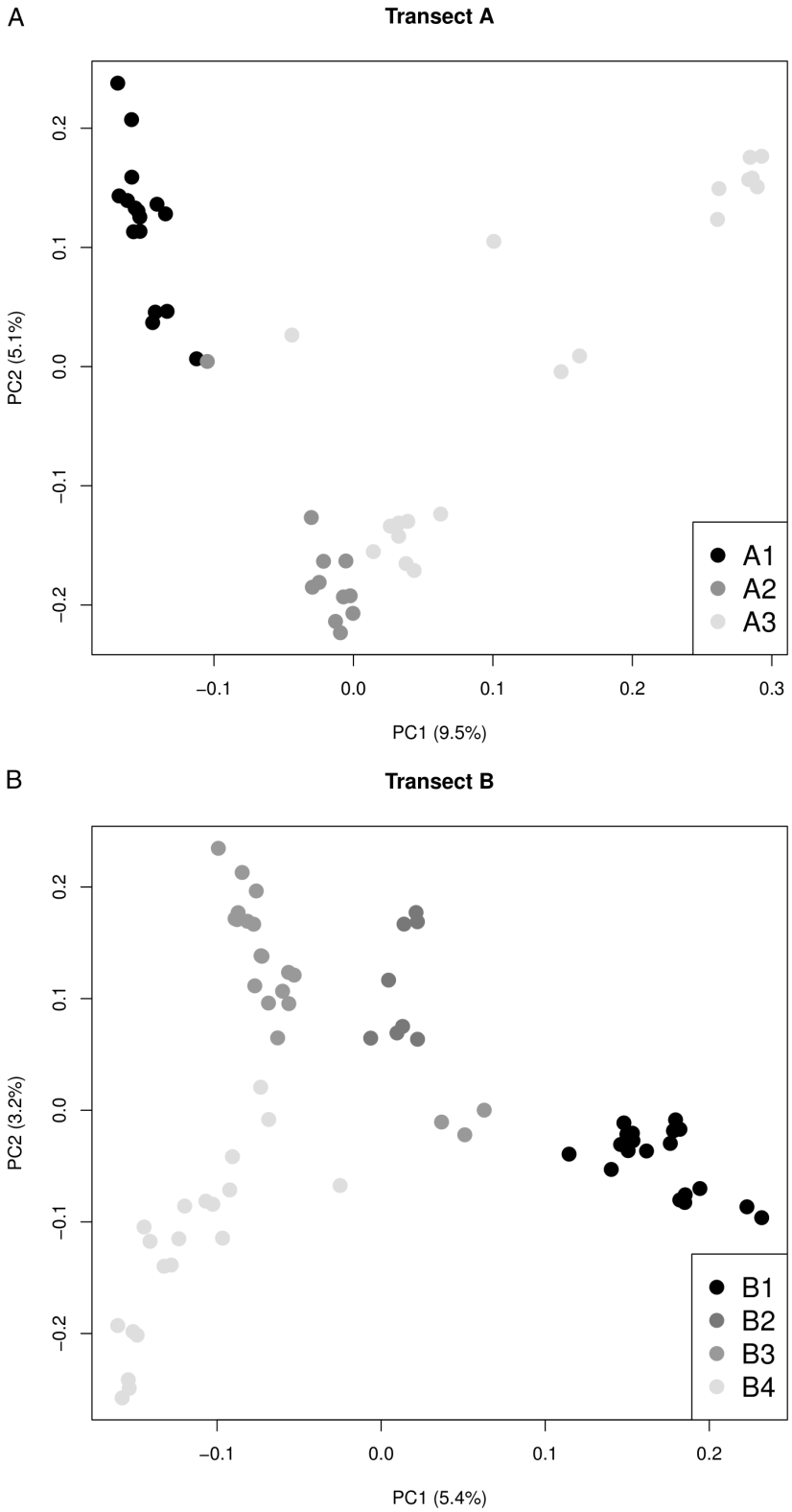

Figure 2. Summary of genetic variation using PCA of 2 *Peromyscus leucopus* lineages north (transect A) and south (transect B) of the St. Lawrence River.

191/281 *LFMM*-outliers in transect A and 83/529 *LFMM*-outliers in transect B are part of the 14 687 "shared SNPs" across transects. Between these shared SNPs that are *LFMM*-outliers (i.e., 191 and 83), we found an overlap of 7 SNPs (Supplementary Table S3). A hypergeometric test showed that an overlap of 7 SNPs is more than expected by chance (P value = 1.2×10^{-5}), considering the number of shared SNPs. However, only 2 of the 7 candidate SNPs have allele frequencies that are in the same direction (increasing)

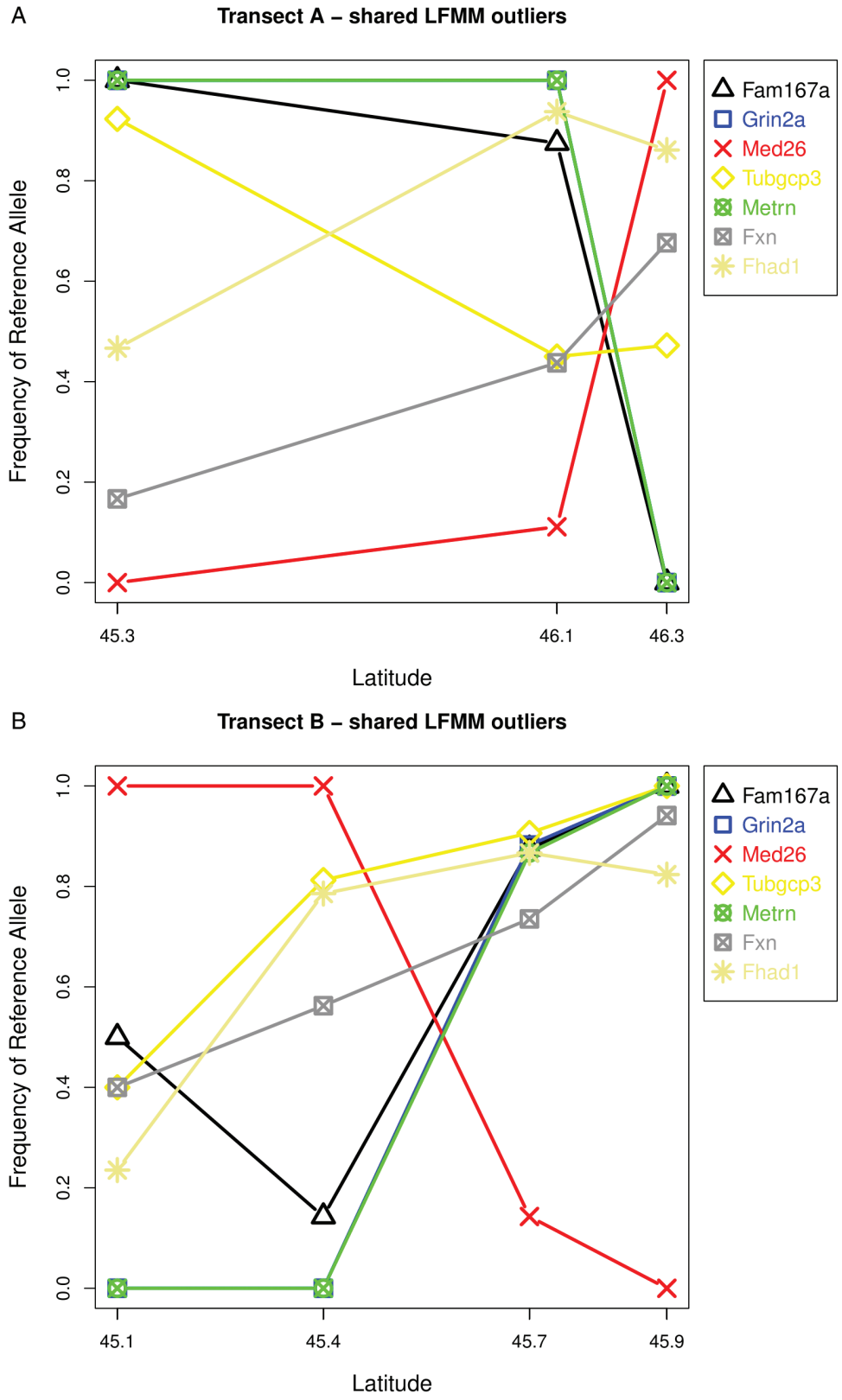

Figure 3. Allele frequencies of 7 genic SNPs (*LFMM*-outliers) found to correlate with climate across 2 *Peromyscus leucopus* lineages. Only 2 candidate genes show parallel allele frequencies (Fxn and Fhad1). See online version for full colors.

in both transects, while the others are anti-parallel (Figure 3). We found that the 2 SNPs that have parallel allele frequencies each map to a different gene, *Fxn* and *Fhad1*. The gene *Fxn* plays a role in protection against iron-induced oxidative stress (O'Neill et al. 2005). Less is known about the function of *Fhad1*, but it contains a region coding for a forkhead-associated domain. Other genes with

forkhead and forkhead-associated domains have functions related to histone H3 modification during the G2/M phase of cell division (Prigent and Dimitrov 2003; Rieder 2011), which is consistent with the putative functional targets of clinal selection found in this study (see *Potential functional roles of candidate SNPs*). In both transects, 3 of the anti-parallel SNPs have opposite alleles fixed at sites representing the limits of the gradient. Two of these map to genes involved in the nervous system (genes *Grin2a* and *Metrn*).

Allele Frequency Clines

Within each transect, we fit a LOESS curve to our *pcadapt-LFMM*-outlier frequencies to visualize how genomic variation putatively under natural selection changes with the environmental gradient (Figure 4). Some outlier SNPs have reference alleles (i.e., major allele) that increase in frequency along the gradient, while other outliers have alleles that decrease in frequency. Notably, in transect B, the 2 smoothed averages of all allele frequencies going in opposite directions have a similar nonlinear shape, sharing a drastic change of allele frequencies at similar latitudinal points, between sites B2 and B3 (Figure 1). Because no significant barrier to dispersal exists between these 2 sites, this pattern supports a role for natural selection, where alleles at different SNPs experience a transition in the selective regime at the same point along the environmental gradient (Vines et al. 2016; Bradley et al. 2017). In transect A, with fewer *pcadapt-LFMM*-outlier SNPs (i.e., wider error bands) and limited to only 3 data points or sites sampled, this pattern is not observed.

SNP Annotation

We assessed the number of genic SNPs and different genes found in our 2 datasets (Supplementary Figures S10 and S11). We find that 63% of SNPs from transect A map to 5140 different protein-coding genes (genic SNPs: 13 563; intergenic SNPs: 7492; mean: 2.6 SNPs per gene). In transect B, 60% of SNPs were found in 9912 different genes (genic SNPs: 47 221; intergenic SNPs: 32 122; mean: 4.8 SNPs per gene). Among *pcadapt-LFMM*-outliers, we find 59% map to 21 different protein-coding genes in transect A (genic outliers: 22; intergenic outliers: 15, Supplementary Table S4). In transect B, we find that 64% of outliers map to 77 different genes (genic outliers: 87; intergenic outliers: 50, Supplementary Table S5), with an additional outlier mapping to a pseudogene and one to a genomic region for long noncoding RNA.

Potential Functional Roles of Candidate SNPs

We hypothesized that selection for climate adaptation in *P. leucopus* on the range margin would be reflected as an enrichment of GO terms relevant to torpor, such as metabolism and behavior. Analysis of candidate genes shows 57 biological processes overrepresented in transect A ($P < 0.05$; Supplementary Table S6) and 123 in transect B ($P < 0.05$; Supplementary Table S7). Our GO analysis finds shared overrepresentation across transects for functions related to glucose homeostasis and synaptic transmission. Additionally, we find an overrepresentation of genes for histone acetylation, the G2/M transition of the cell cycle, and Ca^{2+} transport.

Discussion

We analyzed genome-wide SNPs from *P. leucopus* on the northern range margin to identify SNPs associated with winter climate. We hypothesized that subtle differences in winter climate at the edge of the species distribution would impose selection on physiological and behavioral traits for thermal adaptation, and that this would be reflected as allele frequency changes in genes involved in metabolism and the central nervous system. Consistent with expectations, our results showed evidence of putative clinal selection on genes for glucose metabolism and synaptic transmission. In addition, we found enrichment of gene functions related to H3 histone modification, Ca^{2+} balance, and the G2/M transition of the cell cycle among those genes identified as candidates by both genome scans we implemented. However, the evidence of parallelism at the SNP level was limited, with only 2 SNPs showing parallel clines in allele frequency.

Evidence of Parallel Selection

Parallel evolution is considered strong support for the deterministic effect of natural selection (Rosenblum et al. 2014). We found limited evidence of parallelism across transects, with most candidate SNPs (i.e., *LFMM*-outliers shared between transects A and B) showing anti-parallel patterns of allele frequencies. However, we found that 2 SNPs showed parallel allele frequencies and they mapped to different genes, including a mitochondrial gene (*Fxn*) involved in the protection against iron-dependent oxidative stress (O'Neill et al. 2005). Other mitochondrial genes have been found to have a similar protective function of guarding against iron-dependent oxidative stress during torpor (Wu et al. 2015). The other parallel SNP we found maps to *Fbad1*, a gene containing a forkhead-associated domain. While the function of this particular gene is not known, other genes with forkhead and forkhead-associated domains are known to play important roles at the G2/M check-point of cell division (Prigent and Dimitrov 2003; Rieder 2011). Consistent with this, we found an enrichment of genes with functions at the G2/M transition among candidate genes identified as being under selection by *LFMM*. The forkhead transcription factors *Fox0* protect against oxidative stress and are involved in cell cycle arrest (i.e., quiescence), specifically at the G2/M boundary (Greer and Brunet 2005). Interestingly, there is evidence that *Fox0* transcription factors protect against oxidative stress (Wu and Storey 2014) and inhibit muscle atrophy (Zhang et al. 2016) during torpor. Further functional work is needed to determine whether *Fxn* and *Fbad1* have any functional role in climate adaptation.

There are biological reasons for observing limited parallelism at the SNP level. For example, our finding of less overlap at the SNP level than at the functional level is consistent with the idea that the chance of finding parallel evolution depends on the level of biological hierarchy investigated (Bolnick et al. 2018). Parallel evolution of the mutations or genes is less likely than parallel evolution of phenotypes or fitness due to the redundancy of many-to-one mapping between SNPs, phenotypes, and fitness (Stadler et al. 2001; Thompson et al. 2017). One advantage is that many-to-one mapping allows for functional modularity of traits. For example, 2 cichlid species have independently evolved to graze on algae through parallel evolution of jaw protrusion abilities and 4-bar linkage that arose through nonparallel changes to 4-bar morphologies (Hulsey et al. 2019). A similar functional convergence has been observed in labrid fishes (Alfaro et al. 2004).

Another process that can blur the signature of parallel clinal selection at the SNP level is adaptive introgression (Taylor and Larson 2019). The ecological consequences of climate change, for example, range expansion (Roy-Dufresne et al. 2013), may facilitate the breakdown of reproductive barriers between *P. leucopus* and *P. maniculatus* (Currat et al. 2008; Chunco 2014). Indeed, previous studies have shown evidence of hybridization between these 2 species south of the St. Lawrence River (Leo and Millien 2017; Garcia-Elfring et al. 2017). This hybridization could lead to the introgression of adaptive loci from the more cold-adapted *P. maniculatus* to *P.*

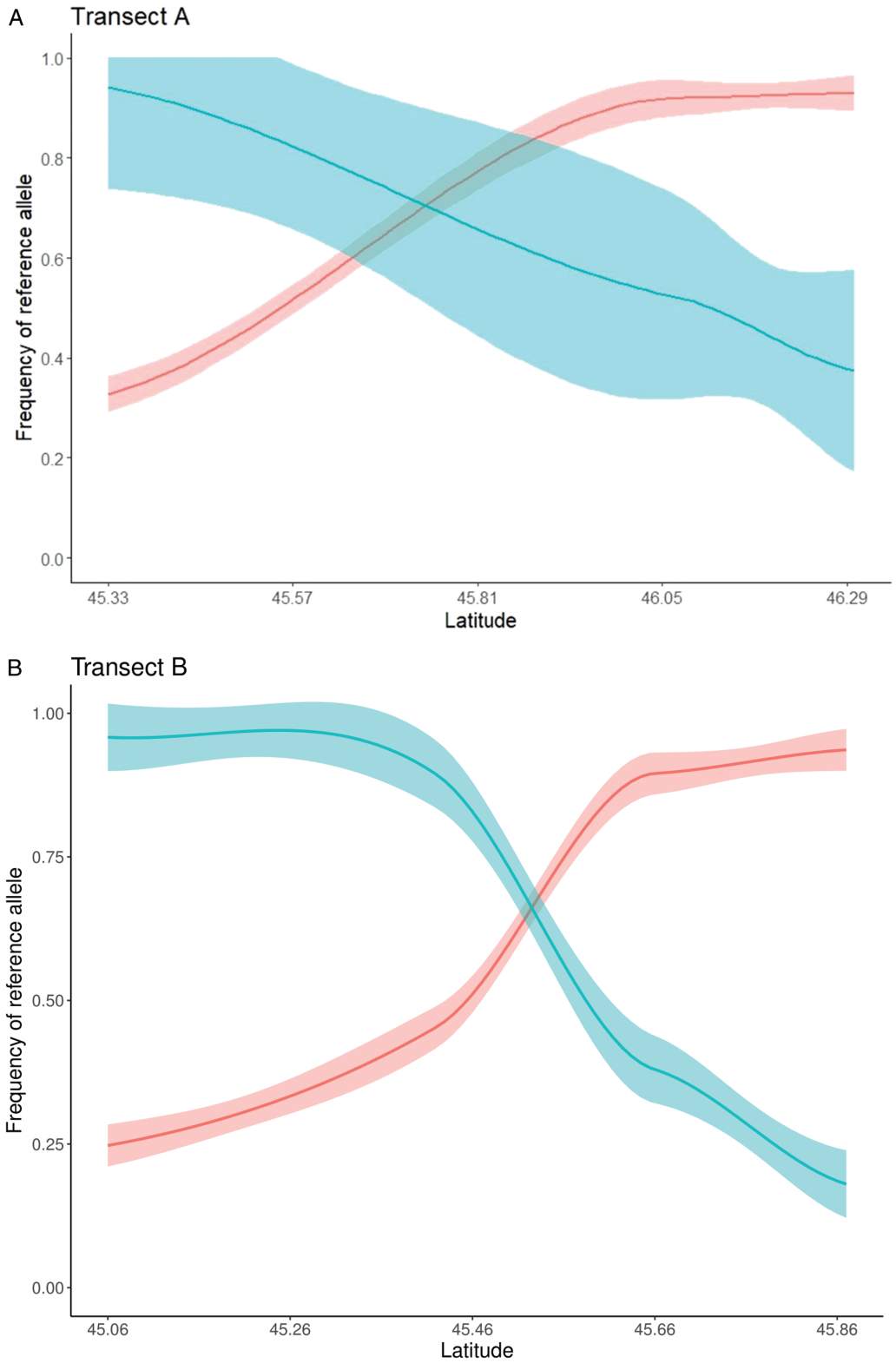

Figure 4. LOESS regression fitted to allele frequencies of *pcadapt-LFMM*-outliers from transect A ($n = 37$) and transect B ($n = 137$). Some outliers have reference (i.e., major) alleles that decrease in frequency along the gradient (blue cline), others increase in frequency (red cline). Lines depict the smoothed trend of allele frequencies and shaded areas represent 95% confidence bands. See online version for full colors.

leucopus. Hybridization between a local and colonizing species can also lead to the replacement of the local species by the colonizer (Rhymer and Simberloff 1996). There is evidence that *P. leucopus* is replacing *P. maniculatus* as the most abundant *Peromyscus* species in some areas of southern Quebec (Millien et al. 2017), although whether hybridization is a factor is not known.

The limited parallelism at the SNP level was also possibly affected by the use of RAD-seq. Because RAD-seq inherently samples only part of the genome, many regions under selection could have been missed. Furthermore, it is also possible that the lack of overlap across transects between *pcadapt-LFMM*-outliers was partly due to the different statistical approaches between *LFMM* and *pcadapt*. While *LFMM* explicitly tests for associations between environmental parameters, *pcadapt* does not. This means that *pcadapt* can detect patterns of allele frequency that are consistent with clinal adaptation, but it will be unclear which specific parameters are responsible. It is possible that *pcadapt* will detect local adaptation to conditions along the cline that are not reflected by the particular environmental factors tested by *LFMM*, and this may result in a lack of overlap between outliers using each method.

Signatures of Selection on Gene Functions with Potential Links to Torpor

Successful overwintering strategies require behaviors appropriate for the thermal environment. For example, differences in nest-building and food-hoarding behaviors in anticipation of winter (Pierce and Vogt 1993) have likely facilitated the establishment of *P. maniculatus* in colder latitudes than *P. leucopus*. We found clinal variation on genes enriched in functions related to the central nervous system, which may be the result of subtle behavioral differences between populations on opposite ends of the gradient. While the genetic basis of overwintering behavior (e.g., extent of added insulation) is not yet known, similar complex traits such as burrow construction (Weber et al. 2013) and reproductive nest building (Bendesky et al. 2017) are known to be controlled by specific genomic regions in some *Peromyscus* species. Our work identifies genomic regions potentially involved in adaptive behavioral responses to local climate.

Mammals that initiate torpor demonstrate a metabolic switch from catabolizing glucose to mainly using lipids for energy (Yan et al. 2008; Melvin and Andrews 2009). Both lineages in this study showed overrepresentation of gene functions in glucose and glycogen metabolism among candidate genes. One of the genes associated with energy balance is linked to obesity in some human populations (gene *Klf9*; Okada et al. 2012). Previous work investigating genomic targets of adaptation to different thermal regimes in humans has found candidate genes linked to common metabolic disorders (Hancock et al. 2008) and nutrient metabolism (Fumagalli et al. 2015). A recent study on *P. leucopus* revealed signatures of selection on genes linked to carbohydrate and lipid metabolism on an urban–rural gradient (Harris and Munshi-South 2017), a gradient which also correlates with temperature. Our results are thus consistent with the literature indicating metabolic changes are important for thermal adaptation in mammals.

Although not predicted a priori, we discovered enrichment of GO terms for H3 histone modification, cell division (G2/M transition), and intracellular Ca^{2+} homeostasis. For example, both lineages shared evidence of selection for genes involved in histone acetylation. These findings are consistent with research on the molecular basis of torpor. Epigenetic mechanisms like histone modification play important roles in the modulation of metabolism during torpor (Morin and Storey 2006; Alvarado et al. 2015; Tessier et al. 2017; Rouble et al. 2018). During the initiation of torpor, a reduction of transcriptional activity in skeletal muscle is associated with deacetylation of histones (Morin and Storey 2006), while histone acetylation is up-regulated in metabolically active brown adipose tissue (Rouble et al. 2018). Modification of H3 histones are known to have functions in the cell cycle, interestingly, during the G2/M phase, and in the suppression of transcription activity (Prigent and Dimitrov 2003). Indeed, there is evidence that H3 histone modification is involved in the suppression of gene transcription during torpor (Zhang et al. 2016).

It is also well known that accompanying a reduction of metabolic activity during hibernation is the cessation of cell division. Mayer and Bernick (1958) documented cellular quiescence in hibernating ground squirrels. More recently, it was shown that genes responsible for cell cycle arrest show an increase in expression during hibernation initiation, while genes promoting cell division increase during arousal from hibernation (Yan et al. 2008; Wu and Storey 2012). Work by Turbill et al. (2012) also documented a difference in telomere length between torpid and nontorpid hamsters. The coupling of cell cycle processes with hibernation may reflect an adaptation against oxidative stress and premature senescence (i.e., cellular aging) during nonreproductive periods of time (Turbill et al. 2012).

Finally, we found an overrepresentation of genes involved in Ca^{2+} homeostasis among SNPs showing strong allele frequency clines. Precise regulation and compartmentalization of intracellular Ca^{2+} have been found to be adaptations for proper heart function (Wang et al. 2002; Yatani et al. 2004; Nakipova et al. 2017) and, interestingly, against muscle atrophy (Cotton 2016; Fu et al. 2016; Guo et al. 2017) during hibernation. Overall, the enrichment of gene functions related to glucose metabolism, neural circuitry, histone modification, cell division, and Ca^{2+} balance suggest that *P. leucopus* on the range margin in southern Quebec have physiological phenotypes linked to torpor under clinal selection.

We note that our analysis only provides indirect inferences about associations of candidate SNPs and adaptive function and fitness (Nielsen 2009; Barrett and Hoekstra 2011; Pavlidis et al. 2012). We are also limited by sample size (i.e., collection sites) in our ability to pick-up clinal signals. This is especially the case in transect A, where we have data from only 3 sites. The role that outlier SNPs found in this study have in climate adaptation should therefore be viewed with caution. With further functional work the link, if any, of our candidate SNPs to climate adaptation can be clarified.

Conclusion

We found signatures of selection reflected as allele frequency clines along a latitudinal gradient, although evidence for parallelism was limited. Our findings suggest that *P. leucopus* populations on the northern range limit have experienced clinal selection for gene functions associated with energy balance, the central nervous system, histone modification, cell division, and intracellular Ca^{2+} regulation. We speculate that these functions play a role in torpor, but further work making the genotype-phenotype-fitness link is needed to reach strong conclusions. Nonetheless, our findings add to our understanding of the genetics of thermal adaptation in small mammals and sheds light on the functional targets of selection expected with climate change.

Supplementary Material

Supplementary data are available at *Journal of Heredity* online.

Funding

This research was funded through NSERC Discovery Grants RGPIN-2017-03839 and RGPIN-2019-04549 to V.M. and R.D.H.B., respectively, and a Canada Research Chair to R.D.H.B.

Acknowledgment

We thank Juntao Hu for helpful advice on the GO enrichment analysis.

Data Accessibility

The raw sequence data has been deposited at the NCBI Short Read Archive (SRA) repository and can be accessed under accession number PRJNA397983.

Author Contributions

A.G.E., R.D.H.B., and V.M. conceived of the research. A.G.E. performed the population genomics and bioinformatics, and wrote the article. All authors participated in revising the article and approved the final version.

References

Alexa A, Rahnenfuhrer J. 2016. topGO: enrichment analysis for Gene Ontology. R package version 2.28.0. CRAN.

Alfaro ME, Bolnick DI, Wainwright PC. 2004. Evolutionary dynamics of complex biomechanical systems: an example using the four-bar mechanism. *Evolution*. 58:495–503.

Alvarado S, Mak T, Liu S, Storey KB, Szyf M. 2015. Dynamic changes in global and gene-specific DNA methylation during hibernation in adult thirteen-lined ground squirrels, *Ictidomys tridecemlineatus*. *J Exp Biol*. 218:1787–1795.

Araújo MB, Ferri-Yáñez F, Bozinovic F, Marquet PA, Valladares F, Chown SL. 2013. Heat freezes niche evolution. *Ecol Lett*. 16:1206–1219.

Babin C, Gagnaire PA, Pavey SA, Bernatchez L. 2017. RAD-seq reveals patterns of additive polygenic variation caused by spatially-varying selection in the American eel (*Anguilla rostrata*). *Genome Biol Evol*. 9:2974–2986.

Barrett RD, Hoekstra HE. 2011. Molecular spandrels: tests of adaptation at the genetic level. *Nat Rev Genet*. 12:767–780.

Bassham S, Catchen J, Lescak E, von Hippel FA, Cresko WA. 2018. Repeated selection of alternatively adapted haplotypes creates sweeping genomic remodeling in stickleback. *Genetics*. 209:921–939.

Beaumont MA, Nichols RA. 1996. Evaluating loci for use in the genetic analysis of population structure. *Proc Biol Sci*. 263:1619–1626.

Bendesky A, Kwon YM, Lassance JM, Lewarch CL, Yao S, Peterson BK, He MX, Dulac C, Hoekstra HE. 2017. The genetic basis of parental care evolution in monogamous mice. *Nature*. 544:434–439.

Bolnick DI, Barrett RD, Oke KB, Rennison DJ, Stuart YE. 2018. (Non)parallel evolution. *Annu Rev Ecol Evol Syst*. 49:303–330.

Bradley D, Xu P, Mohorianu II, Whibley A, Field D, Tavares H, Couchman M, Copsey L, Carpenter R, Li M, *et al.* 2017. Evolution of flower color pattern through selection on regulatory small RNAs. *Science*. 358:925–928.

Catchen J, Hohenlohe PA, Bassham S, Amores A, Cresko WA. 2013. Stacks: an analysis tool set for population genomics. *Mol Ecol*. 22:3124–3140.

Chen Z, Farrell AP, Matala A, Narum SR. 2018. Mechanisms of thermal adaptation and evolutionary potential of conspecific populations to changing environments. *Mol Ecol*. 27:659–674.

Chunco AJ. 2014. Hybridization in a warmer world. *Ecol Evol*. 4:2019–2031.

Combosch DJ, Lemer S, Ward PD, Landman NH, Giribet G. 2017. Genomic signatures of evolution in Nautilus—an endangered living fossil. *Mol Ecol*. 26:5923–5938.

Cotton CJ. 2016. Skeletal muscle mass and composition during mammalian hibernation. *J Exp Biol*. 219:226–234.

Currat M, Excoffier L, Maddison W, Otto SP, Ray N, Whitlock MC, Yeaman S. 2006. Comment on "Ongoing adaptive evolution of ASPM, a brain size determinant in *Homo sapiens*" and "Microcephalin, a gene regulating brain size, continues to evolve adaptively in humans". *Science*. 313:172; author reply 172.

Currat M, Ruedi M, Petit RJ, Excoffier L. 2008. The hidden side of invasions: massive introgression by local genes. *Evolution*. 62:1908–1920.

de Villemereuil P, Frichot É, Bazin É, François O, Gaggiotti OE. 2014. Genome scan methods against more complex models: when and how much should we trust them? *Mol Ecol*. 23:2006–2019.

DeCandia AL, Brzeski KE, Heppenheimer E, Caro CV, Camenisch G, Wandeler P, Driscoll C, vonHoldt BM. 2019. Urban colonization through multiple genetic lenses: the city-fox phenomenon revisited. *Ecol Evol*. 9:2046–2060.

Durinck S, Moreau Y, Kasprzyk A, Davis S, De Moor B, Brazma A, Huber W. 2005. BioMart and Bioconductor: a powerful link between biological databases and microarray data analysis. *Bioinformatics*. 21:3439–3440.

Durinck S, Spellman PT, Birney E, Huber W. 2009. Mapping identifiers for the integration of genomic datasets with the R/Bioconductor package biomaRt. *Nat Protoc*. 4:1184–1191.

Elshire RJ, Glaubitz JC, Sun Q, Poland JA, Kawamoto K, Buckler ES, Mitchell SE. 2011. A robust, simple genotyping-by-sequencing (GBS) approach for high diversity species. *PLoS One*. 6:e19379.

Fiset J, Tessier N, Millien V, Lapointe FJ. 2015. Phylogeographic structure of the white-footed mouse and the deer mouse, two Lyme disease reservoir hosts in Québec. *PLoS One*. 10:e0144112.

François O, Martins H, Caye K, Schoville SD. 2016. Controlling false discoveries in genome scans for selection. *Mol Ecol*. 25:454–469.

Frichot E, François O. 2015. LEA: an R package for landscape and ecological association studies. *Methods Ecol Evol*. 6:925–929.

Frichot E, Mathieu F, Trouillon T, Bouchard G, François O. 2014. Fast and efficient estimation of individual ancestry coefficients. *Genetics*. 196:973–983.

Frichot E, Schoville SD, Bouchard G, François O. 2013. Testing for associations between loci and environmental gradients using latent factor mixed models. *Mol Biol Evol*. 30:1687–1699.

Fristoe TS, Burger JR, Balk MA, Khaliq I, Hof C, Brown JH. 2015. Metabolic heat production and thermal conductance are mass-independent adaptations to thermal environment in birds and mammals. *Proc Natl Acad Sci U S A*. 112:15934–15939.

Fu W, Hu H, Dang K, Chang H, Du B, Wu X, Gao Y. 2016. Remarkable preservation of Ca(2+) homeostasis and inhibition of apoptosis contribute to anti-muscle atrophy effect in hibernating Daurian ground squirrels. *Sci Rep*. 6:27020.

Fumagalli M, Moltke I, Grarup N, Racimo F, Bjerregaard P, Jørgensen ME, Korneliussen TS, Gerbault P, Skotte L, Linneberg A, *et al.* 2015. Greenlandic Inuit show genetic signatures of diet and climate adaptation. *Science*. 349:1343–1347.

Garcia-Elfring A, Barrett RDH, Combs M, Davies TJ, Munshi-South J, Millien V. 2017. Admixture on the northern front: population genomics of range expansion in the white-footed mouse *(Peromyscus leucopus*) and secondary contact with the deer mouse (*Peromyscus maniculatus*). *Heredity (Edinb)*. 119:447–458.

Gilbert KJ, Sharp NP, Angert AL, Conte GL, Draghi JA, Guillaume F, Hargreaves AL, Matthey-Doret R, Whitlock MC. 2017. Local adaptation interacts with expansion load during range expansion: maladaptation reduces expansion load. *Am Nat*. 189:368–380.

Grabek KR, Cooke TF, Epperson LE, Spees KK, Cabral GF, Sutton SC, Merriman DK, Martin SL, Bustamante CD. 2017. Genetic architecture drives seasonal onset of hibernation in the 13-lined ground squirrel. *bioRxiv*. 222307. doi:10.1101/222307.

Greer EL, Brunet A. 2005. FOXO transcription factors at the interface between longevity and tumor suppression. *Oncogene*. 24:7410–7425.

Guo Q, Mi X, Sun X, Li X, Fu W, Xu S, Wang Q, Arfat Y, Wang H, Chang H, *et al.* 2017. Remarkable plasticity of Na+, K+-ATPase, Ca2+-ATPase and SERCA contributes to muscle disuse atrophy resistance in hibernating Daurian ground squirrels. *Sci Rep*. 7:10509.

Haldane JB. 1948. The theory of a cline. *J Genet*. 48:277–284.

Hancock AM, Witonsky DB, Gordon AS, Eshel G, Pritchard JK, Coop G, Di Rienzo A. 2008. Adaptations to climate in candidate genes for common metabolic disorders. *PLoS Genet*. 4:e32.

Harris SE, Munshi-South J. 2017. Signatures of positive selection and local adaptation to urbanization in white-footed mice (*Peromyscus leucopus*). *Mol Ecol*. 26:6336–6350.

Heath HW, Lynch GR. 1983. Intraspecific differences in the use of photoperiod and temperature as environmental cues in white-footed mice *Peromyscus leucopus*. *Physiol Zoo*. 56:506–512.

Hill JK, Griffiths HM, Thomas CD. 2011. Climate change and evolutionary adaptations at species' range margins. *Annu Rev Entomol*. 56:143–159.

Hulsey CD, Alfaro ME, Zheng J, Meyer A, Holzman R. 2019. Pleiotropic jaw morphology links the evolution of mechanical modularity and functional feeding convergence in Lake Malawi cichlids. *Proc Biol Sci*. 286:20182358

Humphries MM, Thomas DW, Speakman JR. 2002. Climate-mediated energetic constraints on the distribution of hibernating mammals. *Nature*. 418:313–316.

Johnston IA, Bennett AF, editors. 2008. *Animals and temperature: phenotypic and evolutionary adaptation*. Vol. 59. New York: Cambridge University Press.

Keller I, Seehausen O. 2012. Thermal adaptation and ecological speciation. *Mol Ecol*. 21:782–799.

Langmead B, Salzberg SL. 2012. Fast gapped-read alignment with Bowtie 2. *Nat Methods*. 9:357–359.

Leo SST, Millien V. 2017. Microsatellite markers reveal low frequency of natural hybridization between the white-footed mouse (*Peromyscus leucopus*) and deer mouse (*Peromyscus maniculatus*) in southern Quebec, Canada. *Genome*. 60:454–463.

Lewontin RC, Krakauer J. 1973. Distribution of gene frequency as a test of the theory of the selective neutrality of polymorphisms. *Genetics*. 74:175–195.

Li H, Handsaker B, Wysoker A, Fennell T, Ruan J, Homer N, Marth G, Abecasis G, Durbin R; 1000 Genome Project Data Processing Subgroup. 2009. The Sequence Alignment/Map format and SAMtools. *Bioinformatics*. 25:2078–2079.

Lotterhos KE, Whitlock MC. 2015. The relative power of genome scans to detect local adaptation depends on sampling design and statistical method. *Mol Ecol*. 24:1031–1046.

Lovegrove BG. 2003. The influence of climate on the basal metabolic rate of small mammals: a slow-fast metabolic continuum. *J Comp Physiol B*. 173:87–112.

Luu K, Bazin E, Blum MG. 2017. pcadapt: an R package to perform genome scans for selection based on principal component analysis. *Mol Ecol Resour*. 17:67–77.

Lyman CP, Willis JS, Malan A, Wang LCH. 1982. *Hibernation and torpor in mammals and birds*. New York: Academic Press.

Marrotte RR, Gonzalez A, Millien V. 2014. Landscape resistance and habitat combine to provide an optimal model of genetic structure and connectivity at the range margin of a small mammal. *Mol Ecol*. 23:3983–3998.

Mayer WV, Bernick S. 1958. Comparative histological studies of the stomach, small intestine, and colon of warm and active and hibernating arctic ground squirrels, *Spermophilus undulatus*. *Anat Rec*. 130:747–757.

Melvin RG, Andrews MT. 2009. Torpor induction in mammals: recent discoveries fueling new ideas. *Trends Endocrinol Metab*. 20:490–498.

Millien V, Ledevin R, Boué C, Gonzalez A. 2017. Rapid morphological divergence in two closely related and co-occurring species over the last 50 years. *Evol Ecol*. 31:847–864.

Money D, Gardner K, Migicovsky Z, Schwaninger H, Zhong GY, Myles S. 2015. LinkImpute: fast and accurate genotype imputation for nonmodel organisms. *G3 (Bethesda)*. 5:2383–2390.

Morin P Jr, Storey KB. 2006. Evidence for a reduced transcriptional state during hibernation in ground squirrels. *Cryobiology*. 53:310–318.

Nakipova OV, Averin AS, Evdokimovskii EV, Pimenov OY, Kosarski L, Ignat'ev D, Anufriev A, Kokoz YM, Reyes S, Terzic A, *et al.* 2017. Store-operated Ca^{2+} entry supports contractile function in hearts of hibernators. *PLoS One*. 12:e0177469.

Nielsen R. 2009. Adaptionism—30 years after Gould and Lewontin. *Evolution*. 63:2487–2490.

Nunziata SO, Weisrock DW. 2018. Estimation of contemporary effective population size and population declines using RAD sequence data. *Heredity (Edinb)*. 120:196–207.

O'Neill HA, Gakh O, Park S, Cui J, Mooney SM, Sampson M, Ferreira GC, Isaya G. 2005. Assembly of human frataxin is a mechanism for detoxifying redox-active iron. *Biochemistry*. 44:537–545.

Okada Y, Kubo M, Ohmiya H, Takahashi A, Kumasaka N, Hosono N, Maeda S, Wen W, Dorajoo R, Go MJ, *et al.*; GIANT Consortium. 2012. Common variants at CDKAL1 and KLF9 are associated with body mass index in east Asian populations. *Nat Genet*. 44:302–306.

Pavlidis P, Jensen JD, Stephan W, Stamatakis A. 2012. A critical assessment of storytelling: gene ontology categories and the importance of validating genomic scans. *Mol Biol Evol*. 29:3237–3248.

Pierce SS, Vogt FD. 1993. Winter acclimatization in *Peromyscus maniculatus gracilis*, *P. leucopus noveboracensis*, and *P. l. leucopus*. *J Mammal*. 74:665–677.

Porcelli D, Butlin RK, Gaston KJ, Joly D, Snook RR. 2015. The environmental genomics of metazoan thermal adaptation. *Heredity (Edinb)*. 114:502–514.

Prigent C, Dimitrov S. 2003. Phosphorylation of serine 10 in histone H3, what for? *J Cell Sci*. 116:3677–3685.

Rezende EL, Bozinovic F, Garland T Jr. 2004. Climatic adaptation and the evolution of basal and maximum rates of metabolism in rodents. *Evolution*. 58:1361–1374.

Rhymer JM, Simberloff D. 1996. Extinction by hybridization and introgression. *Annu Rev Ecol Evol Syst*. 27:83–109.

Rieder CL. 2011. Mitosis in vertebrates: the G2/M and M/A transitions and their associated checkpoints. *Chromosome Res*. 19:291–306.

Rosenblum EB, Parent CE, Brandt EE. 2014. The molecular basis of phenotypic convergence. *Annu Rev Ecol Evol Syst*. 45:203–226.

Rouble AN, Hawkins LJ, Storey KB. 2018. Roles for lysine acetyltransferases during mammalian hibernation. *J Therm Biol*. 74:71–76.

Rousset F. 2008. genepop'007: A complete re-implementation of the genepop software for Windows and Linux. *Mol Ecol Resour*. 8:103–106.

Rousset F. 2019. *Genepop version 4.7.0*.

Rowe KC, Heske EJ, Paige KN. 2006. Comparative phylogeography of eastern chipmunks and white-footed mice in relation to the individualistic nature of species. *Mol Ecol*. 15:4003–4020.

Roy-Dufresne E, Logan T, Simon JA, Chmura GL, Millien V. 2013. Poleward expansion of the white-footed mouse (*Peromyscus leucopus*) under climate change: implications for the spread of Lyme disease. *PLoS One*. 8:e80724.

Sambrook J, Fritsch EF, Maniatis T. 1989. *Molecular cloning: a laboratory manual*. Cold Spring Harbor (NY): Cold Spring Harbor Laboratory Press.

Stadler BM, Stadler PF, Wagner GP, Fontana W. 2001. The topology of the possible: formal spaces underlying patterns of evolutionary change. *J Theor Biol*. 213:241–274.

Stadler BM, Bass AJ, Dabney A, Robinson D. 2018. qvalue: Q-value estimation for false discovery rate control. R package version 2.14.0. Available from: URL https://github.com/jdstorey/qvalue.

Storey JD, Tibshirani R. 2003. Statistical significance for genomewide studies. *Proc Natl Acad Sci U S A*. 100:9440–9445.

Tannenbaum MG, Pivorun EB. 1988. Seasonal study of daily torpor in southeastern *Peromyscus maniculatus* and *Peromyscus leucopus* from mountains and foothills. *Physiol Zool*. 61:10–16.

Taylor SA, Larson EL. 2019. Insights from genomes into the evolutionary importance and prevalence of hybridization in nature. *Nat Ecol Evol*. 3:170–177.

Tessier N, Noël S, Lapointe FJ. 2004. A new method to discriminate the deer mouse (*Peromyscus maniculatus*) from the white-footed mouse (*Peromyscus leucopus*) using species-specific primers in multiplex PCR. *Can J Zool*. 82:1832–1835.

Tessier SN, Luu BE, Smith JC, Storey KB. 2017. The role of global histone post-translational modifications during mammalian hibernation. *Cryobiology*. 75:28–36.

Thompson CJ, Ahmed NI, Veen T, Peichel CL, Hendry AP, Bolnick DI, Stuart YE. 2017. Many-to-one form-to-function mapping weakens parallel morphological evolution. *Evolution*. 71:2738–2749.

Turbill C, Smith S, Deimel C, Ruf T. 2012. Daily torpor is associated with telomere length change over winter in Djungarian hamsters. *Biol Lett*. 8:304–307.

Vines TH, Dalziel AC, Albert AY, Veen T, Schulte PM, Schluter D. 2016. Cline coupling and uncoupling in a stickleback hybrid zone. *Evolution*. 70:1023–1038.

Waldvogel AM, Wieser A, Schell T, Patel S, Schmidt H, Hankeln T, Feldmeyer B, Pfenninger M. 2018. The genomic footprint of climate adaptation in *Chironomus riparius*. *Mol Ecol*. 27:1439–1456.

Wang T, Hamann A, Spittlehouse D, Carroll C. 2016. Locally downscaled and spatially customizable climate data for historical and future periods for North America. *PLoS One*. 11:e0156720.

Wang SQ, Lakatta EG, Cheng H, Zhou ZQ. 2002. Adaptive mechanisms of intracellular calcium homeostasis in mammalian hibernators. *J Exp Biol*. 205:2957–2962.

Weber JN, Peterson BK, Hoekstra HE. 2013. Discrete genetic modules are responsible for complex burrow evolution in *Peromyscus* mice. *Nature*. 493:402–405.

White TA, Perkins SE, Heckel G, Searle JB. 2013. Adaptive evolution during an ongoing range expansion: the invasive bank vole (*Myodes glareolus*) in Ireland. *Mol Ecol*. 22:2971–2985.

Wu CW, Biggar KK, Zhang J, Tessier SN, Pifferi F, Perret M, Storey KB. 2015. Induction of antioxidant and heat shock protein responses during torpor in the gray mouse lemur, *Microcebus murinus*. *Genomics Proteomics Bioinformatics*. 13:119–126.

Wu CW, Storey KB. 2012. Pattern of cellular quiescence over the hibernation cycle in liver of thirteen-lined ground squirrels. *Cell Cycle*. 11:1714–1726.

Wu CW, Storey KB. 2014. FoxO3a-mediated activation of stress responsive genes during early torpor in a mammalian hibernator. *Mol Cell Biochem*. 390:185–195.

Yan J, Barnes BM, Kohl F, Marr TG. 2008. Modulation of gene expression in hibernating arctic ground squirrels. *Physiol Genomics*. 32:170–181.

Yatani A, Kim SJ, Kudej RK, Wang Q, Depre C, Irie K, Kranias EG, Vatner SF, Vatner DE. 2004. Insights into cardioprotection obtained from study of cellular Ca^{2+} handling in myocardium of true hibernating mammals. *Am J Physiol Heart Circ Physiol*. 286:H2219–H2228.

Zerbino DR, Achuthan P, Akanni W, Amode MR, Barrell D, Bhai J, Billis K, Cummins C, Gall A, Girón CG, *et al*. 2017. Ensembl 2018. *Nucleic Acids Res*. 46:754–761.

Zhang Y, Tessier SN, Storey KB. 2016. Inhibition of skeletal muscle atrophy during torpor in ground squirrels occurs through downregulation of MyoG and inactivation of Foxo4. *Cryobiology*. 73:112–119.